where I is the $n \times n$ identity matrix, Θ_1 an $n \times n$ null matrix, and Θ an $n \times m$ null matrix. At this point the standard controllability test[1] would be employed. The following theorem shows that controllability of Eq. (1) can be directly obtained using only the matrices A and B, without setting up system (2).

Theorem: The system $\dot{X}(t) = AX(t) + BU(t)$ is completely controllable if and only if the $n \times (nm)$ matrix

$$g = [B|AB|A^2B| \ldots |A^{n-1}B] \tag{6}$$

has rank n. A, B are constant $n \times n$ and $n \times m$ matrices.

Proof: Form the controllability matrix for Eq. (2) with $Z(t)$, C, D given by Eqs. (3–5)

$$G = [J_0|J_1|J_2| \ldots |J_{2n-1}]_{(2n)\times(2nm)}$$

A straightforward calculation shows that

$$J_{2k} = C^{2k}D = \begin{bmatrix} \Theta \\ A^kB \end{bmatrix} \quad 0 \leq k \leq n-1$$

$$J_{2k+1} = C^{2k+1}D = \begin{bmatrix} A^kB \\ \Theta \end{bmatrix} \quad 0 \leq k \leq n-1$$

Let $R = [J_0|J_2| \ldots |J_{2n-2}]$ and $S = [J_1|J_3| \ldots |J_{2n-1}]$. Clearly the columns of R and S are mutually orthogonal. Therefore, $\text{rank}[G] = \text{rank}[R] + \text{rank}[S] \leq 2n$. Since

$$S = \begin{bmatrix} \Theta_1 & I \\ I & \Theta_1 \end{bmatrix} R$$

$\text{rank}[S] = \text{rank}[R]$. Furthermore, it is clear that $\text{rank}[R] = \text{rank}[g] = r \leq n$. Thus, $\text{rank}[G] = 2r \leq 2n$. By the controllability test of Ref. 1, system (2) is completely controllable if and only if $\text{rank}[G] = 2n$. Therefore, the second-order system is completely controllable if and only if $\text{rank}[g] = n$, where g is defined in Eq. (6).

For linear first-order time-dependent systems, Chang's controllability test[2] can be applied, provided the matrices C, D are sufficiently differentiable. Unfortunately, this test does not readily simplify for second-order time-dependent systems of the form (1).

References

[1] Kalman, R. E., Ho, Y. C., and Narendra, K. S., "Controllability of Linear Dynamical Systems," *Contributions to Differential Equations*, Vol. 1, Wiley, New York, 1962, pp. 189–213.

[2] Chang, A., "An Algebraic Characterization of Controllability," *IEEE Transactions on Automatic Control*, AC-10, 1965, pp. 112–113.

Use of Discrete Sonic Jets as Boundary-Layer Trips in Hypersonic Flow

David R. Stone,* A. M. Cary, Jr.,* and E. L. Morrisette*

NASA Langley Research Center, Hampton, Va.

Nomenclature

k = spherical trip height
m = ratio of jet mass flow per jet to the boundary-layer mass defect between jet centerlines
N_{St} = Stanton number based on freestream conditions
P = pressure
R = Reynolds number per cm
R_k = Reynolds number based on trip height
R_{x_k} = Reynolds number based on distance from leading edge to trip position
R_{x_v} = Reynolds number based on distance from the virtual origin (peak heating)
T = temperature
U = velocity
x_k = distance from leading edge to trip position
y = vertical distance from plate surface

Subscripts

aw = referred to adiabatic wall conditions
e = edge of boundary layer
eff = conditions at effective trip size
j = conditions at jet exit
t = total
w = wall
∞ = freestream

Received November 24, 1969.

* Aerospace Engineer, Applied Fluid Mechanics Section, Aero-Physics Division. Associate Member AIAA.

THE low unit Reynolds numbers and high-transition Reynolds numbers associated with high Mach number wind tunnels often necessitate using roughness trips on models to produce turbulent boundary-layer flow. The required trip size needed to produce turbulent flow near the roughness increases with Mach number until at low hypersonic speeds the roughness size required is approximately twice the boundary-layer thickness.[1,2] Such large roughness sizes can produce undesirable element pressure drag[3] as well as downstream flow distortions.[4] Discrete sonic jets have been suggested[5,6] as a means of tripping boundary layers with negligible intrinsic drag. This Note presents transition and flow-field survey data which indicates sonic jet trips can produce comparable lengths of turbulent flow while significantly reducing the downstream flow distortions.

Transition locations were determined from heat-transfer distributions on a sharp leading-edge (thickness less than 0.003 cm) flat plate at a freestream Mach number of approximately 8.5 (total pressure of 1.38×10^7 N/m^2, and total temperature of 825°K) for the discrete jet and spherical element trips located as shown on the insert of Fig. 1. The spherical trip diameter and jet total pressure (injection rate, m) were chosen such that there was no significant forward movement of transition with increasing sphere size or jet pressure (this trip size is designated as the effective trip,[2]). Examples of heat-transfer data for the present tests, shown in Fig. 1, indicate that the maximum length of turbulent flow for the jet with small injection rates ($m \simeq 0.04$) was not too different from that obtained with the effective spherical trip. As indicated on Fig. 1, the turbulent heating rates for both types of effective trips were similar and had fair agreement with the modified Spalding-Chi[7] prediction.

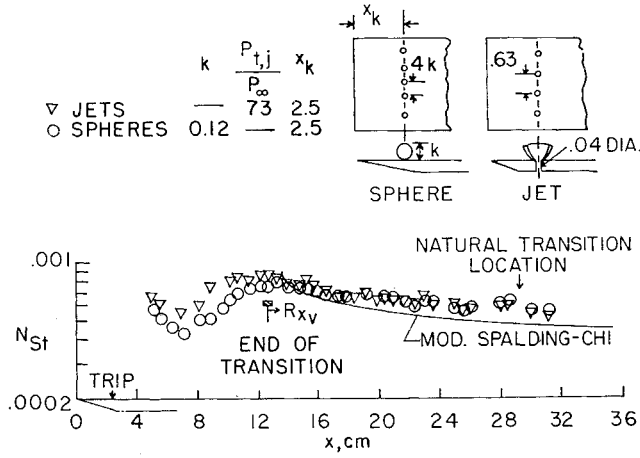

Fig. 1 Heat-transfer distributions for an effective jet and spherical trip showing transition position. $R_\infty = 2.05 \times 10^5$; $T_w/T_t = 0.4$, $m \simeq 0.04$; all dimensions in cm.

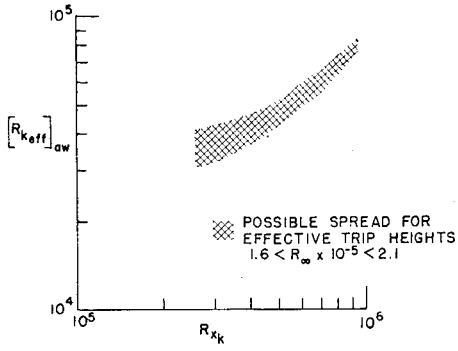

Fig. 2 The effective roughness height Reynolds number for spherical trips, adjusted to adiabatic wall conditions, Mach 8.5.

Flowfield surveys used to evaluate the downstream flow distortions associated with the trips required long test times; thus, the model surface temperatures for the surveys ($T_w/T_t \simeq 0.7$) were higher than for the heat-transfer measurements shown in Fig. 1 ($T_w/T_t = 0.4$). The roughness height and jet pressure were increased so that each trip was effective at the higher wall temperature level. The criterion used to determine the effective spherical trip size for various conditions was based on the effective roughness Reynolds number ($R_{k,\text{eff}}$) and Van Driest's[8] empirical relationship for wall temperature effect as presented in Ref. 2. Effective spherical heights were calculated using the upper portions of the band of Fig. 2 which were obtained using the data of Ref. 2 and unpublished data by the present authors. For the jet trip, it was assumed that an effective penetration height (similar to the spherical roughness height) would also scale according to Van Driest's relationship. Since Refs. 9 and 10 indicate that the jet penetration height and jet normal shock height is approximately proportional to $(P_{t,j}/P_\infty)^{0.5}$, it was further assumed that an effective height of the jet trip would also be proportional to $(P_{t,j}/P_\infty)^{0.5}$ and the jet pressure for the higher wall temperature level was adjusted accordingly.

Downstream total pressure and temperature surveys were made directly behind a tripping element using effective jet and spherical trips. Measured wall static pressure was used to reduce the pitot pressures to Mach number profiles as shown in Fig. 3. Also in Fig. 3 are the no roughness profile (for the inviscid flow) taken at the same location ($x = 28$ cm) and a naturally turbulent boundary-layer profile with the same turbulent Reynolds number (R_{x_v}) taken at $x = 45.5$ cm. The inviscid flowfield in the presence of the jet trip is essentially the same as the flowfield of the no-roughness case. Although the inviscid portion of the flowfield for the spherical roughness placed nearer the leading edge indicates somewhat smaller flowfield disturbances than for the spherical trip

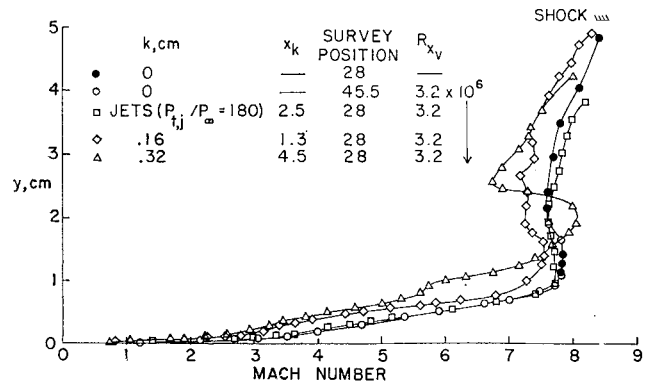

Fig. 3 Effect of trips on downstream flowfield. $R_\infty = 2.05 \times 10^5$; $T_w/T_t \simeq 0.70$; $m \cong 0.06$; all dimensions in cm.

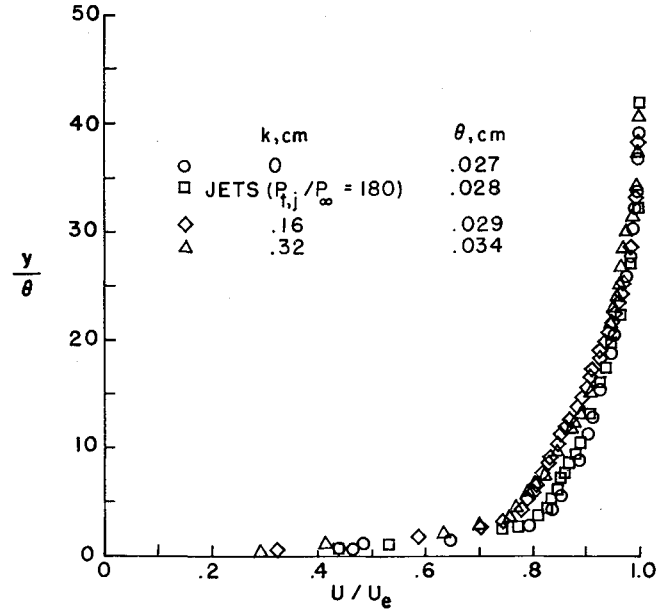

Fig. 4 Effect of trips on boundary-layer velocity profiles. All condition same as for Fig. 3.

placed farther downstream on the plate, neither simulate the natural flowfield to the extent of the jet trip. These flowfield distortions produced by the spherical elements dissipate farther downstream of the roughness; for example, profiles taken at $R_{x_v} = 6.8 \times 10^6$ ($x = 45$ cm), but not presented here, indicate no significant distortions remaining in the inviscid flowfield.

A comparison of the turbulent boundary layer using conventional velocity profiles (calculated from the measured Mach number and temperature profiles) for $R_{x_v} = 3.2 \times 10^6$ is shown in Fig. 4, where the vertical distance has been nondimensionalized by the momentum thickness (θ). Here again, the profile utilizing jet trips better simulates the no-roughness profile taken at the same turbulent Reynolds number (R_{x_v}), especially in the outer regions of the boundary layer. Boundary-layer velocity profiles obtained farther downstream ($R_{x_v} = 6.8 \times 10^6$) of the spherical elements were almost identical to the profile for the jet trip taken at that location.

To summarize, these limited results have indicated that sonic jet trips can induce turbulent flow on wind-tunnel models with no apparent distortions of the downstream flowfield and boundary layer; therefore, jet trips merit serious consideration for tests where trips are needed.

References

[1] Holloway, P. F. and Sterrett, J. R. "Effect of Controlled Surface Roughness on Boundary-Layer Transition and Heat Transfer at Mach Number of 4.8 and 6.0," TN D-2054, April 1964, NASA.

[2] Morrisette, E. L., Stone, D. R., and Whitehead, A. H., Jr., *Boundary-Layer Tripping With Emphasis on Hypersonic Flows*, edited by C. Sinclair Wells, Plenum Press, New York, 1969, pp. 33–51.

[3] Whitehead, A. H., Jr., "Flow Field Studies and Drag Characteristics of Several Boundary-Layer Tripping Elements at Mach 6.8," TN D-5454, Oct. 1969, NASA.

[4] Morrisette, E. L., Stone, D. R., and Cary, A. M., Jr., "Downstream Effects of Boundary-Layer Trips in Hypersonic Flows," *Compressible Turbulent Boundary Layers*, NASA SP 216, 1969, pp. 437–453.

[5] Fage, A., and Sargent, R. F., "An Air-Injection Method of Fixing Transition for Laminar to Turbulent Flow in a Boundary-Layer," R and M 2106, June 1944, Aeronautical Research Council.

[6] Korkegi, R. H., "Transition Studies and Skin-Friction Measurements on an Insulated Flat Plate at a Mach Number of 5.8," *Journal of the Aeronautical Sciences*, Vol. 23, No. 2, Feb. 1956, pp. 97–107.

[7] Bertram, M. H. and Neal, L., Jr., "Recent Experiments in Hypersonic Turbulent Boundary Layers," Presented at the AGARD Specialists Meeting on Recent Developments in Boundary-Layer Research, Naples, Italy, May 1965.

[8] Van Driest, E. R. and Blumer, C. B., "Summary Report on Studies on Boundary-Layer Transition for Years 1963–64," SID 64-2191, Dec. 1964, Space Sciences Lab., North American Aviation Inc.

[9] Zukoski, E. E. and Spaid, F. W., "Secondary Injection of Gases Into a Supersonic Flow," *AIAA Journal*, Vol. 2, No. 10, Oct. 1964, pp. 1689–1696.

[10] Torrence, Marvin, G., "Concentration Measurements of an Injected Gas in a Supersonic Stream," TN D-3860, April 1967, NASA.

Reflected Wave Reverse Flow in an Electromagnetic Shock Tube

David S. Scott*
University of Toronto
AND
Thomas P. Anderson†
University of Iowa

Introduction

Several considerations led us to investigate the possible existence of reverse flow within the plasma generated in a conical electromagnetic shock tube (EMST) after reflection from a downstream bulkhead. These were as follows:

1) Various investigators[1,2] have reported the one-dimensional blast wave behavior of EMST produced flows. Our data was in agreement with these previous observations and, moreover, showed that, after reflection from a downstream bulkhead, the velocity of the reflected luminous front increased with distance from the bulkhead.[3] This increasing velocity had been predicted for one-dimensional blast wave reflection[4] and, hence, its existence further supported the presence of blast wavelike mechanisms within the flows produced by our EMST.

2) If we assume the densities within the wave incident upon the bulkhead resemble those characteristic of a one-dimensional blast wave, the density of the gas into which the reflected plasma moves drops off very rapidly. After the reflected plasma has traveled several diameters from the bulkhead, the density of the incident plasma at the reflected plasma front becomes sufficiently low that there is complete shocked gas diffusion into the reflected plasma. Under these circumstances it is the mass crossing the wave front that is important for determining the velocity behind the wave front, rather than the shock strength as is the case in higher density flows. At this point in the flow it may be assumed, with small error, that the reflected plasma is moving into a vacuum and, hence, that the plasma velocity at the reflected front is equal to the reflected front velocity.

Using standard photomultiplier techniques, reflected luminous front velocities were found to range over 1900–3500 m/sec. depending upon shock tube initial conditions. Therefore, by previous arguments, it was felt that there might exist reverse plasma velocities as high as 3500 m/sec.

3) Makarov and Makismov[5] investigated the thermodynamic state of a plasma after reflection from a downstream bulkhead in a conical EMST and reported temperatures in the order of 13,000°K. It was recognized that temperatures of this order coupled with the plasma velocities indicated by considering 2), suggested that not only should there be a reverse flow but that it might also be supersonic which, if true, could be easily established by image camera photography.

4) Finally, although like many other investigators, we found that in all cases the incident flows exhibited marked instabilities, our data (see Fig. 1) indicated that the reflected plasmas were remarkably stable and reproducible. It was recognized, therefore, that if the reflected wave yielded a supersonic reverse flow its stability would enhance its suitability for a wide range of further studies.

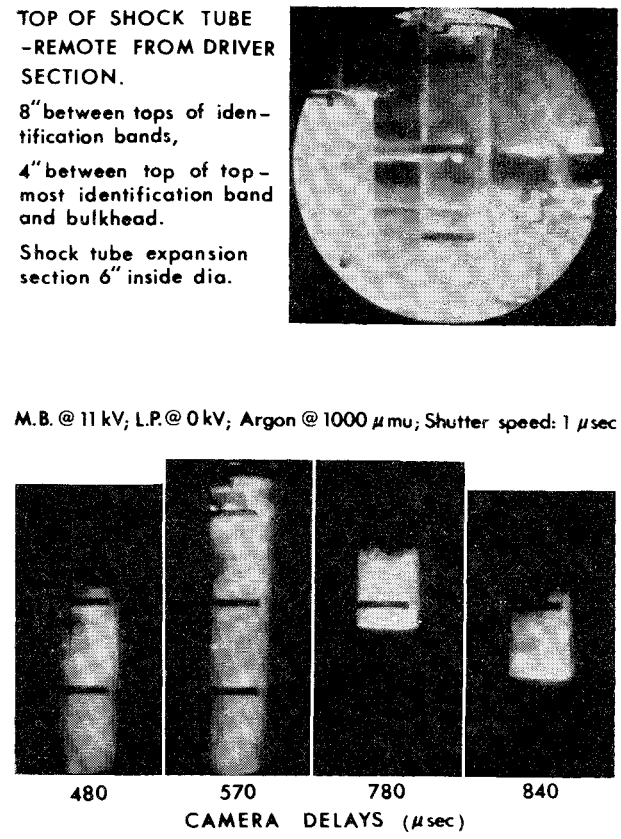

Fig. 1 Sequential development of luminosity.

Facility

The familiar conical driver[2] geometry was chosen. However, to eliminate current streamer wondering and yield a more symmetric energy addition, the usual full-ring electrode was replaced by twelve electrically-isolated electrode-pins, evenly spaced round a shock-tube section and each individually supplied energy from a single 14 μF, 20 kv capacitor. The expansion-section i.d. was 15.25 cm and its length (distance between the bulkhead and the 12 pin-electrode section) was 173 cm. The driver section length (distance between the plane of the 12 pin-electrodes and the tip of the ground electrode) was 59 cm. The EMST had preionize and crowbar capabilities,[3] however, these are unimportant to this note.

Experimental

Image-converter camera and photomultiplier data was used to study the reproducibility, plasma homogeneity and symmetry, of the incident and reflected waves. Figure 1 is representative of a portion of the data.

In all incident front profiles a high degree of asymmetry existed and became even more conspicuous at lower pressures. Our data, however, showed the reflected wave front to be not only symmetric but reasonably planer, with a tendency for

Received November 17, 1969; revision received November 17, 1969.

* Associate Professor of Mechanical Engineering. Member AIAA.

† Professor and Chairman of Mechanical Engineering. Member AIAA.